

Mathematics

Mathematical modeling of monodisperse nanoparticle concentration in aerosols subject to electric field using the Poisson–Nernst–Planck equation

Modelagem matemática da concentração de nanopartículas monodispersas em aerossóis sujeitos a campo elétrico usando a equação de Poisson–Nernst–Planck

Fran Sérgio Lobato ¹ , João Jorge Ribeiro Damasceno ¹ ,
Fabio de Oliveira Arouca ¹ 

¹Universidade Federal de Uberlândia, MG, Brazil

ABSTRACT

In recent decades, the study of particulate materials has gained significant attention from the scientific community. This is due to applications that can be developed, among which we can cite the risks to human health and the environment. As a consequence of this concern, classifying nanoparticles is a topic of considerable interest. One of the most used devices to classify nanoparticles in aerosols is the Differential Mobility Analyzer. From a mathematical point of view, particle concentration profiles have been obtained, preferably, considering constitutive relationships. In this contribution, the Poisson–Nernst–Planck equation is used to determine the concentration of monodisperse nanoparticles in aerosols subjected to an electric field. For this purpose, an inverse problem is proposed and solved considering real data and the Differential Evolution algorithm as an optimization tool. The results demonstrate that the proposed methodology was able to obtain good estimates considering the phenomenological model in relation to experimental points, as well as accurate estimates for intermediate profiles considering the Kriging approach. Finally, it is important to mention that the novelty of this contribution lies in predicting the concentration of monodisperse nanoparticles in aerosols subjected to an electric field using the Poisson–Nernst–Planck equation.

Keywords: Phenomenological model; Nanoparticles separation; Electric field; Inverse problem; Differential Evolution; Kriging

RESUMO

Nas últimas décadas, o estudo de materiais particulados têm atraído a atenção da comunidade científica. Isto se deve as aplicações que podem ser desenvolvidas, entre as quais podemos citar os riscos a saúde humana e ao meio ambiente. Como consequência desta preocupação, a classificação das

nanopartículas configura um tópico de grande interesse. Um dos dispositivos mais utilizados para a classificação de nanopartículas em aerossóis é o Analisador de Mobilidade Diferencial. Do ponto de vista matemático, os perfis de concentração de partículas têm sido obtidos considerando relações constitutivas. Nesta contribuição, a equação de Poisson–Nernst–Planck é empregada para determinar a concentração de nanopartículas monodispersas em aerossóis submetidos a um campo elétrico. Para esta finalidade, um problema inverso é proposto e resolvido considerando dados reais e o algoritmo de Evolução Diferencial como ferramenta de otimização. Os resultados obtidos demonstram que a metodologia proposta foi capaz de obter boas estimativas considerando o modelo fenomenológico em relação aos pontos experimentais, bem como, boas estimativas para perfis intermediários considerando Kriging. Finalmente, é importante mencionar que a novidade desta contribuição é a capacidade de predição da concentração de nanopartículas monodispersas em aerossóis submetidos a um campo elétrico usando a equação de Poisson–Nernst–Planck.

Palavras-chave: Modelo fenomenológico; Separação de nanopartículas; Campo elétrico; Problema inverso; Evolução Diferencial; Kriging

1 INTRODUCTION

Nowadays, the study of nanoparticles is an area of great interest due to their wide range of applications that can be developed, among which we can cite case studies in biotechnology, semiconductor manufacturing, pharmaceuticals, medicine, ceramics, climate change, environment and human health (Gonzalez et al., 2007; Kauffeldt et al., 1995; Lee et al., 2011; Shi et al., 2010; Shu et al., 2005). More recently, due to the importance of applications in catalysis and energy storage, the monodisperse nanoparticles concentration have also gained attention (Camargo et al., 2021; Gomes et al., 2021). As mentioned by Soysal et al. (2017), materials in nano-scale are more easily absorbed by cells, organs, and tissues, by having greater bioavailability, and their toxicity increases with a high surface-to-volume ratio. As a consequence, nanoparticles can cause greater damage to human health and the environment.

In order to evaluate the characteristics of nanoparticles and, consequently, predict aerosol behavior, their size is an important metric. In this case, the particle size can be determined by considering different approaches, such as optical, electrical and combined physical techniques (Kievit et al., 1995). In this scenario, various types of equipment considering particle classification using an electric field can be found. Among them, we can cite the Electrostatically Enhanced Fibrous Filter (EEFF), the

Scanning Mobility Particle Sizer (SMPS), and the Differential Mobility Analyzer (DMA) (Camargo et al., 2021; Gomes et al., 2021; Knight & Petrucci, 2003; Shu et al., 2005).

The mathematical modeling of concentration profiles in these devices is very important because it helps to understand the behavior of nanoparticles and, consequently, corroborates to evaluating parameters and operating conditions that affect the process. Traditionally, models based on transfer functions have been preferentially considered to predict the concentration profiles (Cai et al., 2017; Camargo et al., 2021; Gomes et al., 2021; Hagwood et al., 1999; Karlsson & Martinsson, 2003; Seol et al., 2002; Song et al., 2006). However, the Langevin equation, a phenomenological model, has been used to evaluate the dispersion of ultrafine/nanoparticles in a medium DMA and a Long-DMA (Ramechecandane et al., 2011). Similarly, Ju & Fan (2009) and Salama et al. (2015) investigated a mathematical model for nanoparticle transport in porous and anisotropic media considering experimental data. Dasgupta et al. (2022) evaluated the silica nanoparticle synthesis in a flame spray pyrolysis reactor considering the computational fluid dynamics modeling.

As an alternative to these models, the Poisson–Nernst–Planck (PNP) equation has been considered to represent physical phenomena on a nanometric scale. Lu et al. (2010) proposed an accurate finite element method for solving 3-D PNP equations with singular permanent charges for simulating electrodiffusion in biomolecular systems. Jubery et al. (2012) present the modeling and simulation of nanoparticle separation through a solid-state nanopore. For this purpose, the PNP model is associated with Navier–Stokes equations for fluid flow and on the Langevin equation for particle translocation. Kumaran & Bajpai (2015) present a critical review of the extended Nernst Planck model in the nanofiltration process. In this case, applications involving modeling in nanofiltration for wastewater treatment, heavy metal removal, and charged ion removal are revisited. Cartailier et al. (2017) evaluated the PNP equation for modeling the voltage–current relation in neurobiological microdomains. Jaeger et al. (2023) presented the nano-scale solution of the PNP equations in a fraction of two neighboring cells, revealing the magnitude of intercellular electrochemical waves.

One of the research gaps in this area is due to the lack of studies addressing the PNP equation to estimate monodisperse nanoparticle concentration in aerosols

subject to an electric field. In this case, the present contribution aims to determine a mathematical model based on the PNP equation to represent the monodisperse nanoparticles in aerosol concentration subjected to an electric field in a Nano-Differential Mobility Analyzer (N-DMA). An inverse problem considering real experimental data and the mobility balance is formulated to determine the mass diffusivity and the coefficient of a constitutive model employed to represent the electric potential. To solve the proposed inverse problem, the classical Differential Evolution (DE) algorithm is used as an optimization tool. The novelty of this contribution is not only obtaining a phenomenological model but also estimating the particle concentration profiles considering a set of points related to the concentration of sodium chloride (used to generate the monodisperse solution). For this purpose, a strategy based on the Kriging Interpolation Method (or simply Kriging) is presented.

This work is organized as follows. Section 2 presents the mathematical model that describes the process of interest. Section 3 shows the numerical procedure to integrate the phenomenological model used to represent the physical process. Sections 4 and 5 present a brief description of DE and Kriging, respectively. The proposed methodology is presented in Section 6. The numerical results and discussions are described in Section 7, and the conclusions are outlined in Section 8.

2 MATHEMATICAL MODELING

In this contribution, the concentration of monodisperse nanoparticles in aerosols subjected to an electric field is modeled considering the PNP equation. As mentioned by Masliyah & Bhattacharjee (2006), the PNP equation can be used if the process occurs in a microchannel long where the walls are isolated. As a consequence, the individual ion species for a non-reaction system should be conserved. Mathematically, this model is given by:

$$\frac{\partial C}{\partial t} = -\nabla \cdot j_i \quad (1)$$

where t is the time, C is the concentration of the ion species and j_i is the mass flux of the i -th ion species.

The mass flux can be divided into three contributions (Masliyah & Bhattacharjee, 2006): a convective due to fluid flow, a diffusive part due to Fick's law and a third due to the presence of an electric field. Thus, these contributions can be represented as (Schofer, 2013):

$$j_i = uC - D_i \nabla C + C \omega_i F_{ie} \quad (2)$$

where u is the average velocity, D_i is the mass diffusivity, ω_i is the mobility and F_{ie} is the external force due to the electric field, defined in function of valence (z_i), the fundamental charge of the electron (e) and the potential Ψ , i.e.:

$$F_{ie} = -z_i e \nabla \Psi \quad (3)$$

Thus, the PNP equation can be described as:

$$\frac{\partial C}{\partial t} = -\nabla \cdot (uC - D_i \nabla C + C_i \omega_i z_i e \nabla \Psi) \quad (4)$$

where the electric potential can be calculated by the following model:

$$-\nabla \Psi = \frac{\rho}{\varepsilon} \quad (5)$$

where ρ is the charge density and ε is the electric permittivity. As mentioned by Gomes et al. (2021) and Camargo et al. (2021), the DMA operation depends on the path that particles take inside the analyzer. In this case, it is assumed that the average velocity (u) is given by the following relation (Knutson & Whitby, 1975; Whitby & Clark, 1966):

$$u = \frac{Q}{\pi (r_2^2 - r_1^2)} \quad (6)$$

where Q is the volumetric flow, r_2 and r_1 are the radius of the outer and inner cylinder, respectively. In this case, it is considered that Q is equal to arithmetic mean between the dilution and excess air.

The particle electric mobility can be estimated by (Knutson & Whitby, 1975; Whitby & Clark, 1966):

$$\omega_i = \frac{n\epsilon C_{un}}{3\pi\mu d_p} \quad (7)$$

where n is the number of elementary charge units, C_{un} is the Cunningham slip correction factor, μ is the gas viscosity and d_p is the particle diameter. C_{un} is given by the following relation:

$$C_{un} = 1 + \frac{2\lambda}{d_p} \left(1.115 + 0.471 \exp\left(-0.596 \frac{d_p}{2\lambda}\right) \right) \quad (8)$$

where λ is the mean free path.

As observed in Equation 4, ω_1 and Ψ are dependent on the d_p . Thus, if u , D_i and z_i are constants, the PNP equation in one-dimensional dimension can be written as:

$$\frac{\partial C}{\partial t} = -u \frac{\partial C}{\partial dp} + D_i \frac{\partial^2 C}{\partial dp^2} - z_i e \frac{\partial}{\partial dp} \left(\omega_i C \frac{\partial \Psi}{\partial dp} \right) \quad (9)$$

Expanding the last term and rearranging it, we obtain:

$$\frac{\partial C}{\partial t} = \left(-u - z_i e \omega_i \frac{\partial \Psi}{\partial dp} \right) \frac{\partial C}{\partial dp} + D_i \frac{\partial^2 C}{\partial dp^2} - z_i e \left(\omega_i \frac{\partial^2 \Psi}{\partial dp^2} + \frac{\partial \Psi}{\partial dp} \frac{\partial \omega_i}{\partial dp} \right) C \quad (10)$$

For the sake of simplicity, the above equation can be given as follows:

$$\Omega_1 \frac{\partial C}{\partial t} + \Omega_2 \frac{\partial^2 C}{\partial dp^2} + \Omega_3 \frac{\partial C}{\partial dp} + \Omega_4 C = 0 \quad (11)$$

where

$$\Omega_1 = 1 \quad (12)$$

$$\Omega_2 = -D_i \quad (13)$$

$$\Omega_3 = - \left(-u - z_i e \omega_i \frac{\partial \Psi}{\partial dp} \right) \quad (14)$$

$$\Omega_4 = z_i e \left(\omega_i \frac{\partial^2 \Psi}{\partial dp^2} + \frac{\partial \Psi}{\partial dp} \frac{\partial \omega_i}{\partial dp} \right) \quad (15)$$

The presented model is linear in relation to dependent variable C as the Ω_i ($i=1, \dots, 4$) are constants or functions of the independent variable d_p . The numerical strategy considered to solve this model will be presented in the next section.

3 NUMERICAL PROCEDURE

The phenomenological model addressed in this work was presented in the previous section. This is presented again as follows:

$$\Omega_1 \frac{\partial C}{\partial t} + \Omega_2 \frac{\partial^2 C}{\partial d_p^2} + \Omega_3 \frac{\partial C}{\partial d_p} + \Omega_4 C = 0, \quad 0 \leq t \leq t_f \quad \text{and} \quad 0 \leq d_p \leq d_{p_m} \quad (16)$$

where t_f is the final time and d_{p_m} is the maximum value for the particle diameter.

To integrate this model, the following initial and boundary conditions are considered:

$$C = f(d_p), \quad t = 0 \quad \text{and} \quad 0 \leq d_p \leq d_{p_m} \quad (17)$$

$$\beta_1 C + \beta_2 \frac{\partial C}{\partial d_p} = \beta_3, \quad d_p = 0, \quad t > 0 \quad (18)$$

$$\beta_4 C + \beta_5 \frac{\partial C}{\partial d_p} = \beta_6, \quad d_p = d_{p_m}, \quad t > 0 \quad (19)$$

where f is a function that defines the initial concentration profile, β_s ($s=1, 2, \dots, 6$) is a constant that defines the boundary conditions.

To solve the presented model, the Finite Difference Method (Datta, 2010) is considered. For this purpose, in a d_p -direction, given the interval $[0, d_{p_m}]$, the step size $\Delta d_p = d_{p_m}/M$ (where M and Δd_p are the number of points and the integration step size in the spatial direction, respectively) and the grid points $d_{p_p} = (p-1)\Delta d_p$, $p = 1, \dots, M$. Similarly, in the time direction, given the interval $[0, t_f]$, the step size $\Delta t = t_f/N$ (where N and Δt are the number of points and the integration step size in the temporal direction, respectively) and the grid points $t_k = (k-1)\Delta t$, $k = 1, \dots, N$. In order to represent the differential terms, the following approximations are used (Datta, 2010):

$$\left. \frac{\partial C}{\partial t} \right|_p^k = \frac{C_p^k - C_p^{k-1}}{\Delta t} \quad (20)$$

$$\left. \frac{\partial C}{\partial dp} \right|_p^k = \frac{C_{p+1}^k - C_{p-1}^k}{2\Delta dp} \quad (21)$$

$$\left. \frac{\partial^2 C}{\partial dp^2} \right|_p^k = \frac{C_{p+1}^k - 2C_p^k + C_{p-1}^k}{(\Delta dp)^2} \quad (22)$$

where C_p^k is the value of concentration in a generic point (t_k, dp_p) .

Substituting these approximations into the partial differential equation, we have:

$$\left(\frac{\Omega_2}{(\Delta dp)^2} + \frac{\Omega_3}{2\Delta dp} \right) C_{p+1}^k + \left(\frac{\Omega_1}{\Delta t} - \frac{2\Omega_2}{(\Delta dp)^2} + \Omega_4 \right) C_p^k + \left(\frac{\Omega_2}{(\Delta dp)^2} - \frac{\Omega_3}{2\Delta dp} \right) C_{p-1}^k = \left(\frac{\Omega_1}{\Delta t} \right) C_p^{k-1} \quad (23)$$

This expression is valid for $2 \leq p \leq M-1$ and $2 \leq k \leq N$. For p equal to 1, i.e.; $dp=0$, the derivative is given by:

$$\left. \frac{\partial C}{\partial dp} \right|_{p=1}^k = \frac{C_{p+1}^k - C_p^k}{\Delta dp} \quad (24)$$

Thus, the first boundary condition can be written as:

$$\beta_1 C_1^k + \beta_2 \frac{C_2^k - C_1^k}{\Delta dp} = \beta_3 \rightarrow \left(\beta_1 - \frac{\beta_2}{\Delta dp} \right) C_1^k + \frac{\beta_2}{\Delta dp} C_2^k = \beta_3 \quad (25)$$

Analogously for the second boundary condition ($p = N$, i.e.; $dp = dp_m$), the derivative is given by:

$$\left. \frac{\partial C}{\partial dp} \right|_{p=N}^k = \frac{C_N^k - C_{N-1}^k}{\Delta dp} \quad (26)$$

Thus, the second boundary condition is given by:

$$\beta_4 C_N^k + \beta_5 \frac{C_N^k - C_{N-1}^k}{\Delta dp} = \beta_6 \rightarrow -\frac{\beta_5}{\Delta dp} C_{N-1}^k + \left(\beta_4 + \frac{\beta_5}{\Delta dp} \right) C_N^k = \beta_6 \quad (27)$$

Finally, the initial condition is given by:

$$C_p^1 = f(dp) \tag{28}$$

The discretized equations can be organized as follows:

$$\begin{bmatrix} \Phi_1 & \Phi_2 & 0 & 0 & 0 & \dots & 0 & 0 & 0 & 0 & 0 \\ \Phi_3 & \Phi_4 & \Phi_5 & 0 & 0 & \dots & 0 & 0 & 0 & 0 & 0 \\ 0 & \Phi_3 & \Phi_4 & \Phi_5 & 0 & \dots & 0 & 0 & 0 & 0 & 0 \\ 0 & 0 & \Phi_3 & \Phi_4 & \Phi_5 & \dots & 0 & 0 & 0 & 0 & 0 \\ \vdots & \vdots & \vdots & \vdots & \vdots & \ddots & \vdots & \vdots & \vdots & \vdots & \vdots \\ 0 & 0 & 0 & 0 & 0 & \dots & \Phi_3 & \Phi_4 & \Phi_5 & 0 & 0 \\ 0 & 0 & 0 & 0 & 0 & \dots & 0 & \Phi_3 & \Phi_4 & \Phi_5 & 0 \\ 0 & 0 & 0 & 0 & 0 & \dots & 0 & 0 & \Phi_3 & \Phi_4 & \Phi_5 \\ 0 & 0 & 0 & 0 & 0 & \dots & 0 & 0 & 0 & \Phi_6 & \Phi_7 \end{bmatrix} \begin{bmatrix} C_1^k \\ C_2^k \\ C_3^k \\ C_4^k \\ \vdots \\ C_{N-3}^k \\ C_{N-2}^k \\ C_{N-1}^k \\ C_N^k \end{bmatrix} = \frac{\Omega_1}{\Delta t} \begin{bmatrix} \beta_3 \frac{\Delta t}{\Omega_1} \\ C_2^{k-1} \\ C_3^{k-1} \\ C_4^{k-1} \\ \vdots \\ C_{N-3}^{k-1} \\ C_{N-2}^{k-1} \\ C_{N-1}^{k-1} \\ \beta_6 \end{bmatrix} \tag{29}$$

where:

$$\Phi_1 = \left(\beta_1 - \frac{\beta_2}{\Delta dp} \right) \tag{30}$$

$$\Phi_2 = \frac{\beta_2}{\Delta dp} \tag{31}$$

$$\Phi_3 = \left(\frac{\Omega_2}{(\Delta dp)^2} - \frac{\Omega_3}{2\Delta dp} \right) \tag{32}$$

$$\Phi_4 = \left(\frac{\Omega_1}{\Delta t} - \frac{2\Omega_2}{(\Delta dp)^2} + \Omega_4 \right) \tag{33}$$

$$\Phi_5 = \left(\frac{\Omega_2}{(\Delta dp)^2} + \frac{\Omega_3}{2\Delta dp} \right) \tag{34}$$

$$\Phi_6 = -\frac{\beta_5}{\Delta dp} \tag{35}$$

$$\Phi_7 = \left(\beta_4 + \frac{\beta_5}{\Delta dp} \right) \tag{36}$$

For the k -th time step, the concentration can be determined if the model and numerical method parameters, boundary conditions, and the initial condition (concentration at $(k-1)$ th time step) are known.

4 DIFFERENTIAL EVOLUTION ALGORITHM

The Differential Evolution (DE) algorithm, proposed by Storn & Price (1997) to solve mono-objective optimization problems, is a population-based strategy widely used by the scientific community. More recently, applications in mono- and multi-objective contexts in different fields can be found in the specialized literature (Garcia et al., 2024; Gomes et al., 2021; Lobato et al., 2023; Paes et al., 2022).

In general, the main steps of DE can be summarized as follows (Storn & Price, 1997):

- Initially, an initial population is randomly generated considering NP candidates (formed by a set of design variables). It is important to mention that these design variables should satisfy the domains imposed by the user;
- In its classic configuration, an individual (X_1) is randomly selected in the population to be replaced. Two other individuals (X_2 and X_3), also randomly selected, are used to perform the vector subtraction;
- The result of the subtraction operation is weighed by the perturbation rate (F). This result ($F \times (X_2 - X_3)$) is added to the individual (X_1). Thus, a potential candidate (X) is given by: $X = X_1 + F \times (X_2 - X_3)$. It is important to mention that other strategies to generate potential candidates can be used, as suggested by Storn & Price (1997);
- The vector (X) can replace a previously chosen candidate. For this purpose, a comparison between the crossover probability (CR) (defined by the user) with a random number (r_n) is realized. If r_n is less than CR , this new candidate is accepted. Otherwise, the previously chosen candidate survives in the next generation. This procedure is repeated until a new population is formed.

The presented steps are repeated until the maximum number of generations (defined by the user) is found. More details about this population-based optimization strategy can be found in Storn & Price (1997).

5 KRIGING INTERPOLATION METHOD

In order to increase the prediction capacity of a traditional polynomial model, the mining engineer Danie G. Krige (Krige, 1951) proposed a combination between polynomial and stochastic models applied to the geostatistics field. This approach, called the Kriging Interpolation Method (or simply Kriging), was improved years later by Matheron (1963). However, it was only with a study conducted by Sacks et al. (1989) that this methodology gained prominence as a strategy for modeling engineering systems.

In general terms, Kriging consists of treating the proposed model as capable of representing a stochastic process (Forrester et al., 2008; Gaspar et al., 2014; Hussein & Deb, 2016). For this reason, the mathematical model for Kriging approximation can be represented as:

$$Y(x) = F(x) + Z(x) \quad (37)$$

where $Y(x)$ is the unknown response, $F(x)$ is a simpler function (usually a polynomial function) of independent variable x , and $Z(x)$ is the zero-mean stochastic contribution, with variance σ^2 and non-zero covariance, called correlation functions. These functions can be classified into two groups, one in which the functions have a parabolic behavior close to the origin (Gauss, Cubic and Spline), and the other in which the functions present a linear behavior close to the origin (Exponential, Linear and Spherical). According to Lophaven et al. (2002), the choice of the correlation function should be motivated by the characteristics of the phenomenon analyzed.

In a stochastic model, the change in experimental points presents a random contribution. Thus, modeling a stochastic process in relation to experimental points provides an insight into how this function may behave and how much it tends to change as new points that present different quantities in each coordinate are introduced (Lophaven et al., 2002).

From a mathematical point of view, in a stochastic process, it is assumed that errors are dependent, i.e.; the correlation between errors is related to the distance between the corresponding points. Thus, at this distance (d), the following expression

can be modeled:

$$d(x^i, x^j) = \sum_{k=1}^K \theta_k |x_k^i - x_k^j|^{q_k} \quad (38)$$

where θ and q are vectors of parameters that should be determined.

In Kriging, the random variables are correlated through the following relationship:

$$d(x^i, x^j) = \exp\left(-\sum_{k=1}^K \theta_k |x_k^i - x_k^j|^{q_k}\right) \quad (39)$$

By using Equation 39, the correlation matrix (θ) of all η samples can be determined:

$$\Theta = \begin{pmatrix} \text{correlation}(\eta(x^1), \eta(x^1)) & \cdots & \text{correlation}(\eta(x^1), \eta(x^l)) \\ \vdots & \ddots & \vdots \\ \text{correlation}(\eta(x^l), \eta(x^1)) & \vdots & \text{correlation}(\eta(x^l), \eta(x^l)) \end{pmatrix} \quad (40)$$

and the covariance matrix:

$$\text{Covariance}(\eta, \eta) = \sigma^2 \Theta \quad (41)$$

Considering the correlation and covariance matrix, the vector of parameters (θ and q) can be estimated and, consequently, prediction models considering Kriging can be obtained.

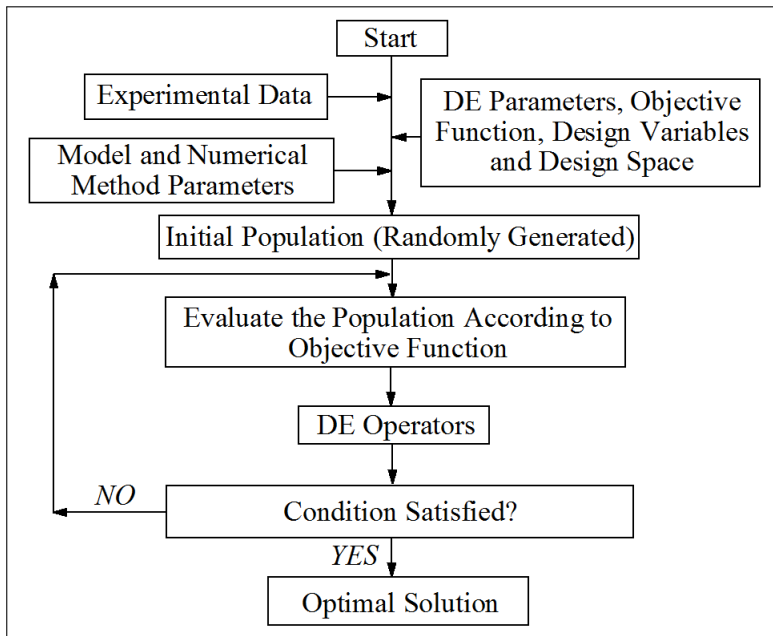
More details about the mathematical development of the Kriging approach can be found in Lophaven et al. (2002).

6 METHODOLOGY

As mentioned earlier, the main aim of this contribution is to determine the mass diffusivity and the coefficients of the proposed approximation for the potential considering the PNP equation and experimental data. For this purpose, a model that represents the mass transfer (Equation 4) and electric potential needs to be integrated (Equation 5). As demonstrated by Gomes et al. (2021) and Camargo et al. (2021), there is a theoretical relationship between the potential and particle diameters. Thus, in this

study, a polynomial approximation will be used to represent this physical quantity. As a consequence, an equation to represent the potential should not be considered, as only the mass transfer model is required.

Figure 1 – Differential Evolution



Caption: Flowchart showing the numerical solving of the proposed inverse problem by using PNP and DE

Source: the authors (2024)

In this case, the proposed inverse problem can be formulated as:

$$\min \text{OF} = \sum_{i=1}^{n_1} \frac{(\Psi_i^{\text{exp}} - \Psi_i^{\text{cal}})^2}{(\max(\Psi^{\text{exp}}))^2} + \sum_{j=1}^{n_2} \frac{(C_j^{\text{exp}} - C_j^{\text{cal}})^2}{(\max(C^{\text{exp}}))^2} \quad (42)$$

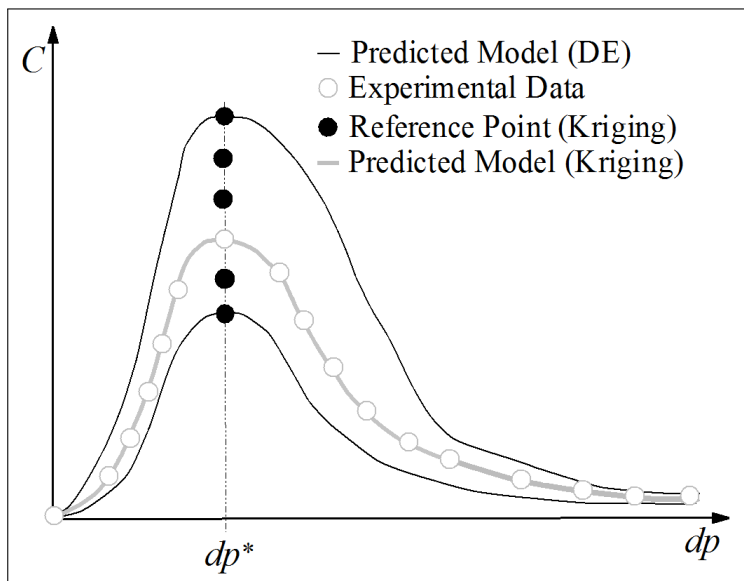
where OF is the objective function, Γ_i^{exp} and Γ_i^{cal} ($\Gamma = \Psi, C$) are the experimental (or theoretical in the case of the potential) and simulated (potential and concentration) profiles, respectively, n_1 and n_2 represent the number of experimental (or theoretical) points for potential and concentration profiles, respectively, and $\max(\Gamma^{\text{exp}})$ is the highest experimental (or theoretical) value observed. To represent the potential, a cubic polynomial function (defined after preliminary tests) is considered:

$$\Psi = \psi_1 dp^3 + \psi_2 dp^2 + \psi_3 dp + \psi_4 \quad (43)$$

where ψ_i ($i=1, 2, \dots, 4$) is the set of design variables that should be determined, as well as the mass diffusivity in the PNP equation.

A flowchart showing the numerical solving of the proposed inverse problem considering the PNP equation and DE algorithm is presented in Figure 1.

Figure 2 – Kriging strategy



Caption: Flowchart for numerical approximation by using Kriging and predicted models by using DE
Source: the authors (2024)

As observed in Camargo et al. (2021), three concentrations of sodium chloride were considered to produce nanoparticles. As a consequence, three experimental monodisperse flows were obtained. In order to estimate the concentration of monodisperse flow in other concentrations for sodium chloride, the Kriging approach, associated with predicted profiles by using DE, is considered. This strategy is presented in Figure 2 and is summarized in the following points:

- Initially, the monodisperse flow profiles (Predicted Models (DE)) with limit concentrations (highest and lowest concentrations of sodium chloride) obtained by DE are used to define a set of points considered during the Kriging application.
- For each value of dp^* belonging to interval $[0, dp_m]$, the concentrations of monodisperse flow limit (computed by the Predicted Models (DE)), as well as reference points (Kriging) are the input parameters in Kriging. Thus, for a given

concentration of sodium chloride, the Predicted Model (Kriging) estimates the value of the monodisperse flow concentration.

- After repeating this process for all dp values, the profile estimated by the Predicted Model (Kriging) is compared with the experimental points to verify the quality of the obtained prediction.

It is important to mention that this strategy aims to predict the monodisperse flow concentration profiles for any concentration of sodium chloride (within the limits established in the experimental procedure) considering the obtained profiles for solving an inverse problem.

7 RESULTS AND DISCUSSION

In order to apply the proposed methodology, the following points should be highlighted:

- To formulate the inverse problem, the experimental points for concentration of monodisperse flow and the theoretical points for the potential obtained by Camargo et al. (2021) considering an N-DMA were considered. The nanoparticles were produced considering a solution comprising ultra-pure water (solvent) and aqueous solutions of sodium chloride (NaCl). For this purpose, the following concentrations of sodium chloride were considered: 0.01 g/L, 0.1 g/L and 0.2 g/L.
- To obtain the experimental points, the following parameters/operational conditions were considered (Camargo et al., 2021): polydisperse flow (0.5 L/min), monodisperse flow (0.5 L/min), sheath flow (5 L/min), excess flow (5 L/min), length (23.5 cm), radii of the inner cylinder (1.5 cm) and radii of the outer cylinder (4.9 cm), air viscosity ($1,83 \times 10^{-5} \text{ kgm}^{-1}\text{s}^{-1}$), a fundamental charge of the electron (1.6×10^{-19} Coulomb), mean free path (0.067 μm). In the N-DMA, voltages considered were defined in the range from 0 to 5000 V. In this case, the particle diameter in the monodisperse flow ranged from 10 to 120 nm. Thus dp_m is equal to 120 nm in all simulations. The final time (t_f) is equal to 1000 s (based on the experimental procedure conducted by Camargo et al. (2021)).

- To integrate the PNP equation, a mesh with $[N \times M]=[100 \times 100]$ points along with the t and dp were used (parameters chosen from preliminary simulations). In this case, points equally spaced in space and time were considered. As the discretized model is linear and tridiagonal, for each time step, the Thomas algorithm (Datta, 2010) is considered as a strategy to solve the model obtained from the discretization process.
- The initial condition considered to integrate the PNP equation is given as: $f(dp)=0$. This condition can be easily justified because if t is equal to zero, there are no particles inside the N-DMA. The boundary conditions were defined based on the experimental profiles presented by Camargo et al. (2021), i.e.; for dp equal to zero, the particle concentration is zero. On the other hand, for dp equal to dp_m , the mass flow is equal to zero.
- To solve each inverse problem, the following parameters were used by the DE algorithm: 50 individuals, the perturbation rate and probability crossover equal 0.8, respectively, 250 generations. In this case, the computational cost, in each run of the optimization algorithm, is equal to $50+50 \times 250$ objective function evaluations. Each inverse problem was run 10 times to obtain both the average values and standard deviation.
- The design space for this problem was defined as: $-10 \leq \psi_i \leq 10$ ($i=1, 2, \dots, 4$) and $10^{-12} \leq D_i \leq 10^{-6}$. It is important to mention that the range for potential was determined after the preliminary runs. In addition, the range for mass diffusivity was based on values observed in the literature (Dasgupta et al., 2022; Jaeger et al., 2023; Ju & Fan, 2009; Jubery et al., 2012).
- The association between quadratic and Gauss strategies was considered a correlation function in all simulations performed by Kriging.
- To compute the CPU time, all simulations were carried out by using Scilab software (version 6.1.1), considering a microcomputer Intel(R) Core(TM) i7-4770K CPU 3.50GHz with 8GB RAM and a 64-bit operation system.

7.1 Inverse Problem

Table 1 presents the average value and the standard deviation for each estimated parameter considering three concentrations of sodium chloride ([0.01 0.1 0.2] g/L). Given the value of the standard deviation corresponding to each parameter, it is clear that the proposed methodology is robust in the sense of estimating the model parameters for the analyzed data set. This can also be observed for the value of the obtained objective function (OF) in each inverse problem. Regarding the processing time (τ), it can be observed that this value is related to the number of runs required by the DE algorithm, i.e.; for each potential candidate, the model for N points discretized in time and for M points discretized in space need to be integrated. This process is repeated along the generations considered, resulting in obtained processing time. Regarding mass diffusivity, its value reduces when the concentration of sodium chloride is increased.

Table 1 – Numerical results

Concentration of sodium chloride (0.01 g/L)						
D_i (nm ² /s)	ψ_1 (V/nm ³)	ψ_2 (V/nm ²)	ψ_3 (V/nm)	ψ_4 (V)	OF	τ (s)
6.151×10^{-9} *	-6.912×10^{-4}	3.219×10^{-1}	-1.922×10^{-1}	2.542×10^{-2}	1.189×10^{-1}	3542
3.599×10^{-11} **	1.232×10^{-8}	4.965×10^{-7}	1.943×10^{-8}	8.967×10^{-8}	7.574×10^{-1}	444
Concentration of sodium chloride (0.1 g/L)						
D_i (nm ² /s)	ψ_1 (V/nm ³)	ψ_2 (V/nm ²)	ψ_3 (V/nm)	ψ_4 (V)	OF	τ (s)
3.489×10^{-9}	-6.924×10^{-4}	3.111×10^{-1}	-1.807×10^{-1}	2.566×10^{-2}	2.223×10^{-1}	3644
7.998×10^{-11}	2.343×10^{-8}	7.876×10^{-7}	1.454×10^{-9}	2.321×10^{-8}	2.324×10^{-4}	258
Concentration of sodium chloride (0.2 g/L)						
D_i (nm ² /s)	ψ_1 (V/nm ³)	ψ_2 (V/nm ²)	ψ_3 (V/nm)	ψ_4 (V)	OF	τ (s)
2.107×10^{-9}	-6.922×10^{-4}	3.222×10^{-1}	-1.920×10^{-1}	2.555×10^{-2}	5.574×10^{-1}	3873
1.908×10^{-11}	1.222×10^{-9}	1.544×10^{-8}	1.889×10^{-9}	4.662×10^{-8}	1.404×10^{-3}	587

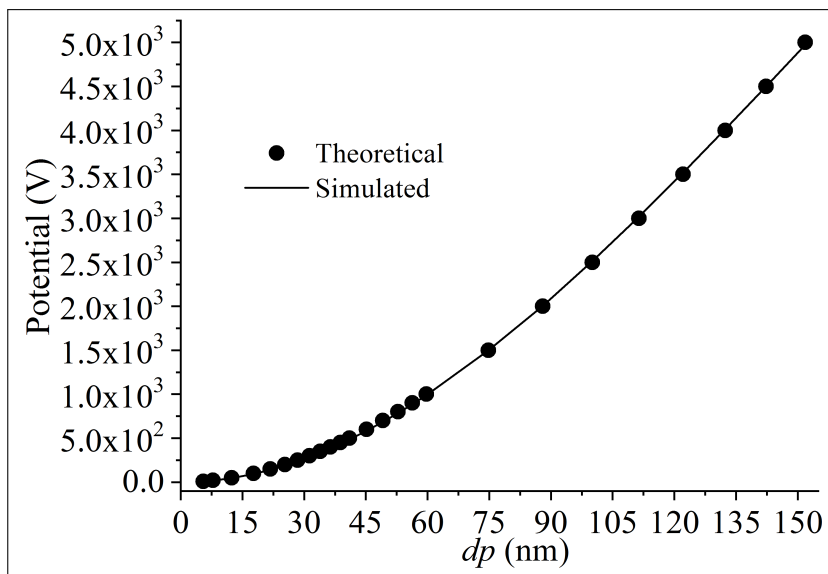
Caption: Design variables, objective function (OF), and processing time (τ) obtained considering each proposed inverse problem. *Average value and **Standard deviation

Source: the authors (2024)

Figure 3 presents the theoretical and simulated profiles. Visually, we can observe an excellent agreement between the theoretical data and those simulated by the polynomial approximation considered. This is due to the smooth behavior between the potential and the diameter. From a physical point of view, it can be

observed that a rise in the potential value implies an increase in the range of particles collected by the classification slit, as mentioned and discussed by Camargo et al. (2021) and Gomes et al. (2021).

Figure 3 – Potential profile



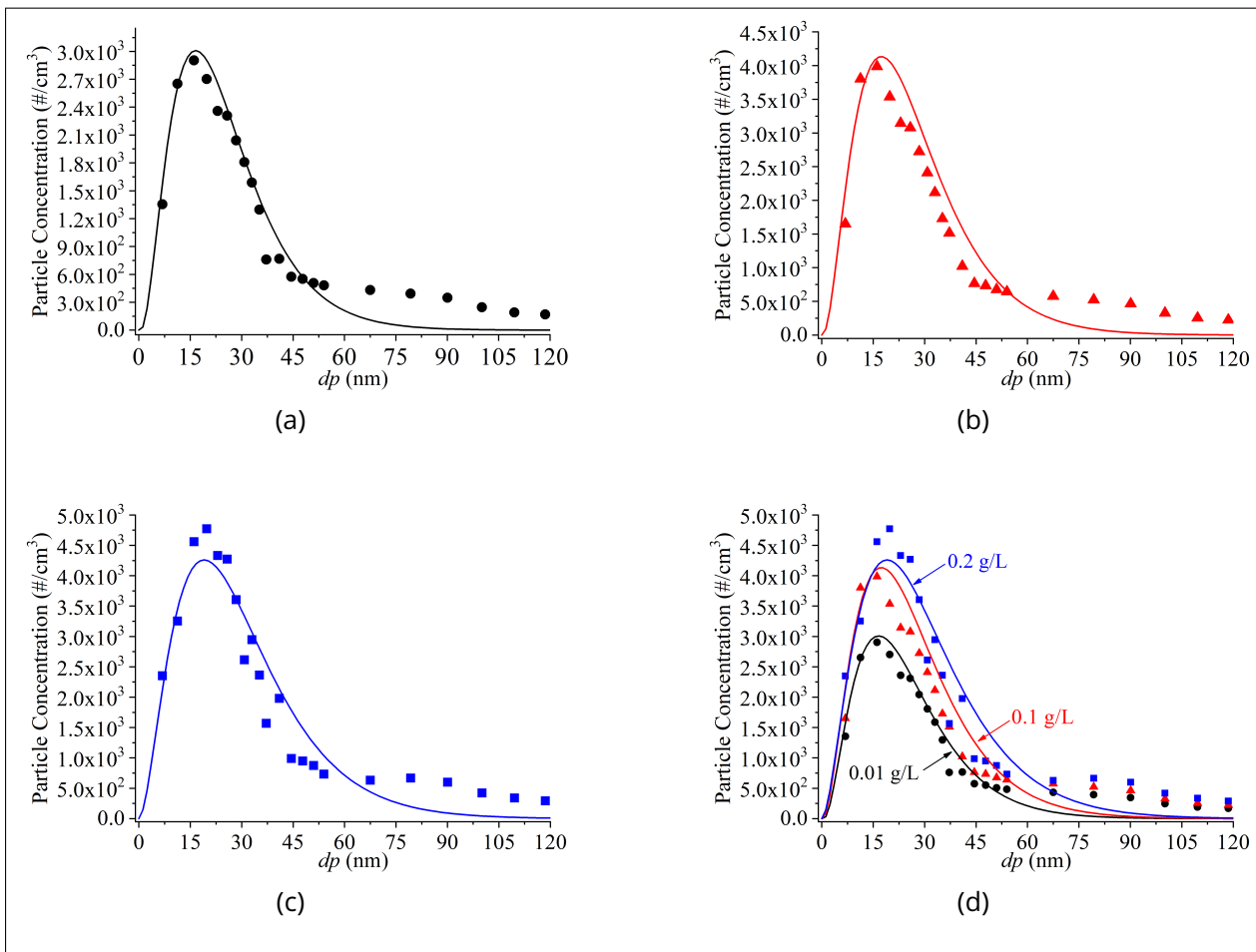
Caption: Theoretical and simulated electric potential

Source: the authors (2024)

Figure 4 shows the simulated profiles of the PNP model at the final time for all the concentrations of sodium chloride ([0.01 0.1 0.2] g/L) compared with the experimental data reported by Camargo et al. (2021). In each figure, the set of estimated parameters may result in good agreement with the dynamics of the physical profile. The obtained values for the objective function considering each inverse problem (see Table 1) corroborates the similarity between the concentration profiles and the analyzed data.

As observed in Figure 4, the monodisperse flow presents a maximum height at a given diameter (related to a given potential); in other words, for this d_p , we obtained the highest particle concentration through the classification slit. Finally, in Figure 4(d), we can observe that the increase in the value of sodium chloride concentration implies an increase in the peak value obtained for the monodisperse flow profile. This was already expected as the increase in the concentration of sodium chloride implies an increase in the number of nanoparticles present in the solution that feeds the N-DMA.

Figure 4 – Experimental and simulated monodisperse flow considering different concentrations of sodium chloride.



Caption: (a) 0.01 g/L, (b) 0.1 g/L, (c) 0.2 g/L and (d) all concentrations

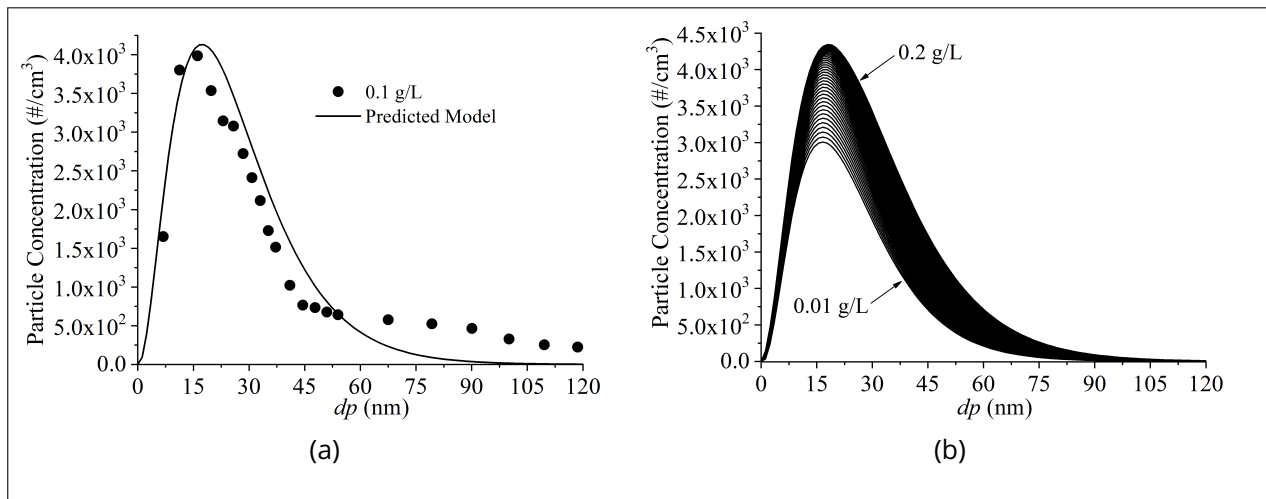
Source: the authors (2024)

7.2 Prediction of Concentration Profile at 0.1 g/L

Figure 5(a) presents the simulated profiles for the concentration profile at 0.1 g/L by using the predicted models for solving two inverse problems (0.01 g/L and 0.2 g/L), i.e., for each concentration of sodium chloride, a different model was computed by using the DE algorithm (see Table 1). In this case, to evaluate the capacity of prediction of the proposed methodology, the obtained concentration of monodisperse flow is compared with experimental data (Camargo et al., 2021). In general, a good capacity of prediction can be observed for the Kriging procedure in relation to experimental data. Similarly, Figure 5(b) presents the concentration of monodisperse flow profiles considering different concentrations of sodium chloride in intervals [0.01 0.2] (g/L). In this case, all concentrations of sodium chloride [0.01 0.1 0.2] (g/L) were

used for this purpose. As observed in this figure, a good capacity of prediction considering the Kriging procedure is obtained in this range. This demonstrates that the proposed methodology to estimate the monodisperse flow profiles in different values of concentrations of sodium chloride resulted in good approximations.

Figure 5 – Estimated monodisperse flow considering the Kriging approach



Caption: (a) Experiment versus predicted model and (b) 0.01-0.2 g/L

Source: the authors (2024)

8 CONCLUSIONS

In this work, an inverse problem to simulate the concentration of nanodisperse flow considering the PNP equation and different values for the concentration of sodium chloride was proposed and solved. For this purpose, the theoretical and experimental points obtained by Camargo et al. (2021) were used to determine the mass diffusivity and the potential by using DE. In order to estimate the particle concentration profile for different values of the base solution, the Kriging approach was associated with predicted models by using DE. The obtained results demonstrate that the proposed methodology was able to obtain good estimates for all concentration profiles when compared with theoretical and experimental data. In addition, the Kriging approach was able to estimate the nanodisperse flow profiles considering the predicted models obtained by using DE.

As mentioned earlier, empirical models based on transfer functions and the Langevin equation have been used to represent the concentration of monodisperse

nanoparticles in aerosols subjected to an electric field (Cai et al., 2017; Camargo et al., 2021; Gomes et al., 2021; Hagwood et al., 1999; Karlsson & Martinsson, 2003; Ramechecandane et al., 2011; Seol et al., 2002; Song et al., 2006). In this context, the use of a more complex model (the PNP equation) represents an advancement over simpler models (transfer functions and the Langevin equation). Although solving the PNP equation requires more computational time, the results obtained from this model account for the effects of convective, diffusive, and electric field terms. This constitutes the main advantage of the proposed methodology.

Finally, it is important to highlight that the use of mathematical modeling associated with the prediction of the monodisperse flow concentration in aerosols can be explained by the difficulty of carrying out countless experiments, whether due to the time dedicated or the cost required. Thus, knowledge of these profiles can contribute to the broad discussion about the potential risks of these nanoparticles to the environment and human health.

For future work, we intend to simulate this physical process considering the Langevin equation, the type-Poisson equation to obtain the potential profile and computational fluid dynamics to determine the velocity profile.

ACKNOWLEDGEMENTS

Dr. Lobato acknowledges the Brazilian agency CNPq for the financial support to his research through the award of a research scholarship (grant number 309178/2023-1).

REFERENCES

Cai, R., Chen, D. R., Hao, J., & Jiang, J. (2017). A miniature cylindrical differential mobility analyzer for sub-3 nm particle sizing. *Journal of Aerosol Science*, 4(106):111–119.

Camargo, E. C. M., Lobato, F. S., Damasceno, J. J. R., & Arouca, F. O. (2021). Experimental and numerical study of monodisperse nanoparticles concentration in a nano-differential mobility analyzer. *Brazilian Journal of Chemical Engineering*, 4(38):389–401.

- Cartailler, J., Schuss, Z., & Holcman, D. (2017). Analysis of the poisson–nernst–planck equation in a ball for modeling the voltage–current relation in neurobiological microdomains. *Physica D*, 4(339):39–48.
- Dasgupta, D., Pal, P., Torelli, R., Som, S., Paulson, N., Libera, J., & Stan, M. (2022). Computational fluid dynamics modeling and analysis of silica nanoparticle synthesis in a flame spray pyrolysis reactor. *Combustion and Flame*, 5(236):111789–111895.
- Datta, B. N. (2010). *Numerical Linear Algebra and Applications*. (2nd ed.). Society for Industrial and Applied Mathematics.
- Forrester, A. I. J., Sobester, A., & Keane, A. J. (2008). *Engineering Design via Surrogate Modelling: A Practical Guide*. John Wiley & Sons Ltd, West Sussex.
- Garcia, V. A., Finzi-Neto, R. M., Lobato, F. S., & Vieira, L. G. M. (2024). Reliability-based design of high-performance hydrocyclones: Multi-objective optimization, fabrication using 3d-printing and experimental analysis. *Powder Technology*, 4(435):119427–119440.
- Gaspar, B., Teixeira, A. P., & Soares, C. G. (2014). Assessment of the efficiency of kriging surrogate models for structural reliability analysis. *Probabilistic Engineering Mechanics*, 4(37):24–34.
- Gomes, T. L. C., Lobato, F. S., Borges, L. C., Damasceno, J. J. R., & Arouca, F. O. (2021). Mathematical modeling of monodisperse nanoparticle production in aerosols using separation in an electric field. *Soft Computing*, 5(25):11347–11362.
- Gonzalez, D., Nasibulin, A. G., Jiang, H., & Queipo, P. (2007). Electro spraying of ferritin solutions for the production of monodisperse iron oxide nanoparticles. *Chemical Engineering Communications*, 5(194):901–912.
- Hagwood, C., Sivathanu, Y., & Mulholland, G. (1999). The dma transfer function with brownian motion a trajectory/monte-carlo approach. *Aerosol Science and Technology*, 5(30):40–61.

- Hussein, R. & Deb, K. (2016). A generative kriging surrogate model for constrained and unconstrained multi-objective optimization. In Friedrich, T. (ed.). *Proceedings of the Genetic and Evolutionary Computation Conference* (pp. 573-580). Association for Computing Machinery.
- Jaeger, K. H., Ivanovic, E., Kucera, J. P., & Tveito, A. (2023). Nano-scale solution of the poisson-nernst-planck (pnp) equations in a fraction of two neighboring cells reveals the magnitude of intercellular electrochemical waves. *PLOS Computational Biology*, 2(19):1–31.
- Ju, B. & Fan, T. (2009). Experimental study and mathematical model of nanoparticle transport in porous media. *Powder Technology*, 11(192):195–202.
- Jubery, T. Z., Prabhu, A. S., Kim, M. J., & Dutta, P. (2012). Modeling and simulation of nanoparticle separation through a solid-state nanopore. *Electrophoresis*, 4(33):325–333.
- Karlsson, M. N. A. & Martinsson, B. G. (2003). Methods to measure and predict the transfer function size dependence of individual dmas. *Journal of Aerosol Science*, 1(34):603–625.
- Kauffeldt, T., Kleinwechter, H., & Schmidt-Ott, A. (1995). Absolute on-line measurement of the magnetic moment of aerosol particles. *Chemical Engineering Communications*, 1(151):169–185.
- Kievit, O., Weiss, M., Verheijen, P. J. T., Marijnissen, J. C. M., & Scarlett, B. (1995). The on-line chemical analysis of single particles using aerosol beams and time of flight mass spectrometry. *Chemical Engineering Communications*, 1(151):79–100.
- Knight, M. & Petrucci, G. A. (2003). Study of residual particle concentrations generated by the ultrasonic nebulization of deionized water stored in different container types. *Analytical Chemistry Journal*, 5(75):4486–4492.
- Knutson, E. & Whitby, K. (1975). Aerosol classification by electric mobility: Apparatus, theory, and applications. *Journal of Aerosol Science*, 4(6):443–451.

- Krige, D. (1951). A statistical approach to some basic nine valuation problems on the witwaters-rand. *Journal of the Chemical, Metallurgical and Mining Engineering Society of South Africa*, 6(52):119–139.
- Kumaran, M. & Bajpai, S. (2015). Application of extended nernst planck model in nano filtration process –a critical review. *International Journal of Engineering Research and Reviews*, 3(3):40–49.
- Lee, H., You, S., Pikhitsa, P. V., Kim, J., Kwon, S., Woo, C. G., & Choi, M. (2011). Three-dimensional assembly of nanoparticles from charged aerosols. *Nano Letters*, 11(1):119–124.
- Lobato, F. S., Alamy-Filho, J. E., Libotte, G. B., & Platt, G. M. (2023). Optimizing breast cancer treatment using hyperthermia: a single and multi-objective optimal control approach. *Applied Mathematical Modelling*, 4(127):96–118.
- Lophaven, S. N., Nielsen, H. B., & Sondergaard, J. (2002). *DACE - A MATLAB Kriging Toolbox*. Version 2.0, Technical University of Denmark, DK-2800 Kgs. Lyngby – Denmark, 1st edition.
- Lu, B., Holst, M. J., McCammond, J. A., & Zhou, Y. C. (2010). Poisson–nernst–planck equations for simulating biomolecular diffusion–reaction processes i: Finite element solutions. *Journal of Computational Physics*, 4(229):6979–6994.
- Masliyah, J. H. & Bhattacharjee, S. (2006). *Electrokinetic and Colloid Transport Phenomena*. John Wiley & Sons.
- Matheron, G. (1963). Principles of geostatistics. *Economic Geology*, 2(58):1246–1266.
- Paes, L. E. S., Andrade, J. R., Lobato, F. S., Santos, M. E., Ponomarov, V., Souza, F. J., & Vilarinho, L. O. (2022). Sensitivity analysis and multi-objective optimization of tungsten inert gas (tig) welding based on numerical simulation. *International Journal of Advanced Manufacturing Technology*, 3(1):1–15.

- Ramechecandane, S., Beghein, C., Allard, F., & Bombardier, P. (2011). Modelling ultrafine/nano particle dispersion in two differential mobility analyzers (m-dma and l-dma). *Building and Environment*, 3(46):2255–2266.
- Sacks, J., Welch, W. J., Mitchell, T. J., & Wynn, H. P. (1989). Design and analysis of computer experiments. *Statistical Science*, 4(4):409–423.
- Salama, A., Negara, A., Amin, M. E., & Sun, S. (2015). Numerical investigation of nanoparticles transport in anisotropic porous media. *Journal of Contaminant Hydrology*, 5(181):114–130.
- Schofer, S. (2013). *Numerical Solution of the Poisson-Nernst-Planck Equation System*. Friedrich-Alexander University of Erlangen-Nuremberg.
- Seol, K. S., Yabumoto, J., & Takeuchi, K. (2002). A differential mobility analyzer with adjustable column length for wide particle-size range measurements. *Journal of Aerosol Science*, 3(33):1481–1492.
- Shi, J., Votruba, A. R., Farokhzad, O. C., & Langer, R. (2010). Nanotechnology in drug delivery and tissue engineering: From discovery to applications. *Nano Letters Journal*, 2(10):3223–3230.
- Shu, J., Wilson, K. R., Arrowsmith, A. N., Ahmed, M., & Leone, S. R. (2005). Light scattering of ultrafine silica particles by vuv synchrotron radiation. *Nano Letters Journal*, 6(5):1009–1015.
- Song, D. K., Lee, H. M., Chang, H., Kim, S. S., Shimada, M., & Okuyama, K. (2006). Performance evaluation of long differential mobility analyzer (ldma) in measurements of nanoparticles. *Journal of Aerosol Science*, 3(37):598–615.
- Soysal, U., Gehin, E., Algre, E., Berthelot, B., Da, G., & Robine, E. (2017). Aerosol mass concentration measurements: Recent advancements of real-time nano/micro systems. *Journal of Aerosol Science*, 1(114):573–586.

Storn, R. & Price, K. (1997). Differential evolution – a simple and efficient heuristic for global optimization over continuous spaces. *Journal of Global Optimization*, 11(1):341–359.

Whitby, K. T. & Clark, W. E. (1966). Electric aerosol particle counting and size distribution measuring system for the 0.05 to 1 μm size range. *Tellus*, 18(1):573–586.

Author contributions

1 – Fran Sérgio Lobato (Corresponding Author)

Chemical Engineer

<https://orcid.org/0000-0002-7401-4718> • fslobato@ufu.br

Contribution: Conceptualization; Literature Review; Methodology; Writing – Original Draft Preparation

2 – João Jorge Ribeiro Damasceno

Chemical Engineer

<https://orcid.org/0000-0002-8146-2092> • damasceno@ufu.br

Contribution: Data Analysis, Writing – Review & Editing

3 – Fabio de Oliveira Arouca

Chemical Engineer

<https://orcid.org/0000-0002-2832-1370> • arouca@ufu.br

Contribution: Data Analysis, Writing – Review & Editing

How to cite this article

Lobato, F. S., Damasceno, J. J. R., & Arouca, F. de O. (2025). Mathematical modeling of monodisperse nanoparticle concentration in aerosols subject to electric field using the Poisson–Nernst–Planck equation. *Ciência e Natura*, Santa Maria, v. 47, e88532. DOI: <https://doi.org/10.5902/2179460X88532>.